tvst

https://doi.org/10.1167/tvst.8.2.15

Article

Relationship Between the Shift of the Retinal Artery Associated With Myopia and Ocular Response Analyzer Waveform Parameters

Shotaro Asano[1], Ryo Asaoka[1], Takehiro Yamashita[2], Shuichiro Aoki[1], Masato Matsuura[1,3], Yuri Fujino[1,3], Hiroshi Murata[1], Shunsuke Nakakura[4], Yoshitaka Nakao[5], and Yoshiaki Kiuchi[5]

[1] Department of Ophthalmology, Graduate School of Medicine and Faculty of Medicine, The University of Tokyo, Tokyo, Japan
[2] Kagoshima University Graduate School of Medical and Dental Sciences, Kagoshima, Japan
[3] Department of Ophthalmology, Graduate School of Medical Sciences, Kitasato University, Kanagawa, Japan
[4] Department of Ophthalmology, Saneikai Tsukazaki Hospital, Hyogo, Japan
[5] Department of Ophthalmology and Visual Science, Hiroshima University, Hiroshima, Japan

Correspondence: Ryo Asaoka, Department of Ophthalmology, Graduate School of Medicine and Faculty of Medicine, The University of Tokyo, Tokyo, Japan. e-mail: rasaoka-tky@umin.ac.jp

Received: 16 October 2018
Accepted: 21 January 2019
Published: 9 April 2019

Keywords: myopia; corneal biomechanics; Ocular Response Analyzer

Citation: Asano S, Asaoka R, Yamashita T, Aoki S, Matsuura M, Fujino Y, Murata H, Nakakura S, Nakao Y, Kiuchi Y. Relationship between the shift of the retinal artery associated with myopia and ocular response analyzer waveform parameters. Trans Vis Sci Tech. 2019;8(2):15, https://doi.org/10.1167/tvst.8.2.15

Purpose: We have recently reported that the retinal stretch due to myopia is closely related to the peripapillary retinal arteries angle (PRAA) (Yamashita et al., *Invest Ophthalmol Vis Sci* 2013;54:5481–5488). The purpose of the current study was to investigate the relationship between retinal artery position and Ocular Response Analyzer (ORA) waveform parameters.

Methods: In 43 eyes of 41 healthy subjects, ORA measurements were carried out and the PRAA was calculated from fundus photographs. Then, the variables related to PRAA were identified from 40 variables of age, axial length (AL), keratometry, ORA corneal hysteresis (CH), ORA corneal resistant factor (CRF), and 35 ORA waveform parameters, using the Lasso regression and model selection with the second-order bias-corrected Akaike information criterion index.

Results: The optimal model for PRAA included AL, CRF, and three ORA waveform parameters (aindex, w2, and slew1). This optimal model was significantly better than the model with AL-only, the model only with AL and CH, and the model only with AL and CRF ($P < 0.0001$, $P < 0.0001$, $P < 0.0001$, respectively; analysis of variance).

Conclusions: The PRAA was significantly better represented by using AL and ORA parameters including waveform parameters, compared with AL alone, with AL and CH alone, and with AL and CRF alone.

Translational Relevance: ORA waveform, which represents corneal biomechanical properties, was associated with myopic retinal stretch.

Introduction

Myopia is one of the major public health concerns, and its effect on retinal pathological changes has gained growing interest.[1] The global prevalence of myopia has increased rapidly in the past 50 years, especially in east and southeast Asia.[1–4] In Japan, the Tajimi study has revealed that the incidence of myopia in the Japanese population was the highest in the world, with an incidence of 41.8% for myopia less than −0.5 diopters (D) and 5.5% for myopia less than −6.0 D in individuals 40 years or older.[5] High myopia has been reported to be related to the increased risks of various manifest ocular diseases, such as choroidal neovascularization,[6] retinal detachment,[7] macular hole,[8] cataract,[9] and glaucoma.[10]

During myopia, the retina is stretched around the papillomacular bundle, and the positions of the peak circumpapillary retinal nerve fiber layer (cpRNFL)

thickness and also retinal arteries are shifted; the supratemporal and inferotemporal RNFL bundles and retinal arteries are shifted closer to the fovea in eyes with longer axial lengths (ALs).[11–13] However, we have recently reported that the correlations between AL and the angles of the cpRNFL peak and retinal artery were merely moderate ($r = -0.49$ and -0.38, respectively).[11] This is because there is a large individual variation in AL at birth, and hence, the degree of retinal elongation cannot be totally explained by AL.[14] For example, we often see paradoxical eyes with a short AL with apparent myopic fundus changes, such as for conus, elliptic optic disc, and smaller peak angle despite short AL.

Recently, it has become possible to measure optical biomechanical properties using Ocular Response Analyzer (ORA; Reichert Inc., Depew, NY) and Corvis Scheimpflug Technology (CST; Oculus, Wetzlar, Germany). We reported that the ability to absorb the applied external energy (hysteresis), as measured with CST biomechanical parameters, was significantly associated with myopic retinal stretch estimated by the cpRNFL peak angle.[15] Another previous study reported that the maximum deformation amplitude measured by CST was associated with the size of β-zone parapapillary atrophy,[16] which has been reported to be associated with the development, severity, progression, and location of glaucoma.[17–20] Our recent studies also suggested that CST parameters were associated with the activity and prognosis of angioid streaks,[21] and also the severity[22] and progression[23] of glaucoma. However, a different study reported no relationship between ORA-measured corneal hysteresis (CH) and β-zone parapapillary atrophy.[24] It is now possible to evaluate corneal biomechanical properties in more detail using ORA by directly analyzing its waveform parameters, and we have reported ORA waveform parameters were superior in evaluating glaucomatous progression compared with the ORA-CH method.[25]

The purpose of the current study was therefore to investigate the relationship between ORA waveform parameters and retinal artery position in eyes with non-high myopia.

Methods

Subjects

The study protocol was approved by the institutional review board of the University of Tokyo Hospital and adhered to the tenets of the Declaration of Helsinki. Written informed consent was obtained from each subject.

Normative eyes, such as eyes screened for glaucoma, fellow eyes of retinal detachment, fellow eyes of traumatic cataract, who had ORA measurement at the University of Tokyo, University of Hiroshima, or Tsukazaki Hospital during the period between January 2016 and December 2017 were retrospectively reviewed, and 43 eyes of 41 subjects with no known eye diseases as determined by examining their medical histories were enrolled. Eligible criteria were as follows: (1) no pathological findings by slit-lamp microscopy, ophthalmoscopy, and/or optical coherence tomography (OCT); (2) best-corrected visual acuity was ≤ 0.1 logarithm of the minimal angle of resolution (logMAR) units; (3) spherical equivalent refractive error (SERE) ≥ -6 D; and (4) intraocular pressure was $\leq$21 mm Hg as measured using Goldmann applanation tonometry. Criteria for exclusion were as follows: (1) known ocular diseases such as glaucoma, staphyloma, and optic disc anomalies; (2) systemic diseases such as hypertension and diabetes; (3) the presence of visual field defects; and/or (4) a history of refractive or any intraocular surgery.

Measurements of AL, Central Corneal Thickness, and Refractive Error

AL was measured using the optical biometer (OA-2000; Tomey, Nagoya, Japan). Central corneal thickness was measured with CST. Refractive error was measured with the Topcon KR8800 autorefractometer/keratometer (Topcon, Tokyo, Japan), and the SERE was calculated.

Peripapillary Retinal Arteries Angle (PRAA)

Optic disc color fundus photographs were obtained using either optical coherence tomography (OCT-2000; Topcon) or a retinal camera (TRC-50DX; Topcon). ImageJ software (https://imagej.nih.gov/ij/; provided in the public domain by the National Institutes of Health, Bethesda, MD) was used to draw a 3.4-mm-diameter peripapillary scan circle on the obtained fundus photographs. The center of the scan circle, which was located at the center of the optic disc, was defined as the intersection point of vertical and horizontal radius lines of the circle. Magnification effects of the camera were corrected using Littmann's formula.[26] Using the scan circle and points where the circle and the center of the superotemporal/infratemporal major retinal artery intersected, the angle between the supratemporal and

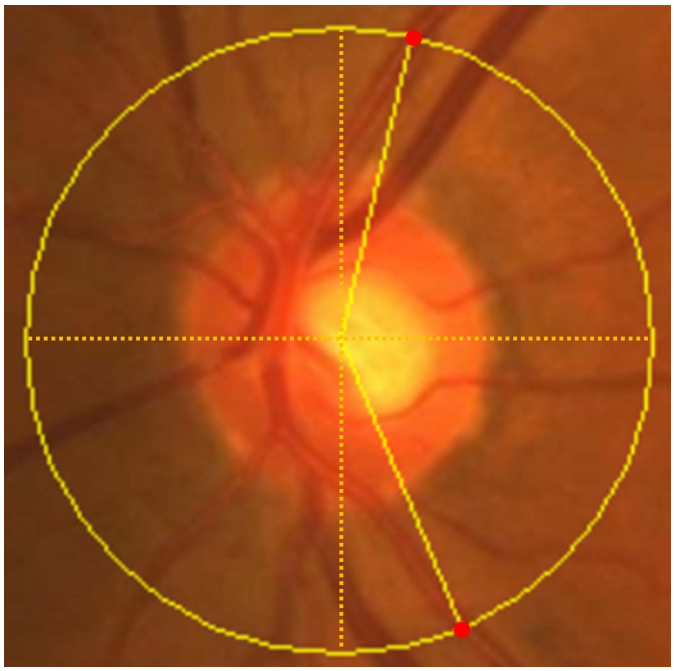

Figure 1. Measurement of PRAA (left eye). The PRAA was calculated by identifying the intersecting positions (*red dots*) of a 3.4-mm-diameter peripapillary scan circle (*yellow*) and the supratemporal/infratemporal major retinal artery, and the angle between the supratemporal and infratemporal major retinal artery. The center of the optic disc was defined as the intersection point of vertical and horizontal diameters of the circle (*yellow dotted lines*). The right eye was mirror-imaged.

infratemporal major retinal artery was measured (PRAA) (Fig. 1).

Ocular Response Analyzer

The details of the ORA measurement were described previously.[27] Briefly, the ORA records two applanation pressures, before and after an indentation of the cornea with the application of a rapid air jet. Due to its viscoelastic property, the cornea resists the air puff, resulting in a delay in the outward corneal movement, which causes the difference in the pressures at the inward and outward applanation. This difference is called CH.[28] The CRF is also calculated using the difference between the inward and outward pressure, but indicates the elastic property of the cornea.[29] The ORA waveform is composed of two peaks, the in-signal peak (peak 1) and out-signal peak (peak 2); each represents inward and outward applanation events, respectively. The ORA waveform parameters consist of 35 parameters that represent characteristics of the two ORA response wave peaks. These parameters are defined as height (h1 and h2), width (w1, w2, w11, and w21), degree (uslope1, uslope2, uslope11, uslope21, dslope1, dslope2, dslope11, dslope21, slew1, and slew2), length (mslew1, mslew2, dive1, dive2, path1, path2, path11, and path21), area (p1area, p2area, p1area1, and p2area1), aspect ratio (aspect1, aspect2, aspect11, and aspect21), and the degree of non-monotonicity (aindex and bindex) of the two peaks, and frequency noise between the two peaks (aplhf), as illustrated in Figure 2. The ORA measurements were carried out three times with at least a 5-minute interval between each measurement, and the average value was used in the analysis. All data had a quality index of more than 7.5 as recommended by the manufacturer.

Statistical Analysis

The relationships between the PRAA and the 40 variables of age, AL, keratometry, CH, CRF, and the 35 ORA waveform parameters were evaluated, using two-step feature selections, because of a large number (40) of analyzed variables. Two ORA waveform parameters of h11 and h21 were not used, because they are in a complete interchangeable relationship (correlation coefficient = 1.0) with h1 and h2. First, 20 candidate variables were selected using least absolute shrinkage and selection operator (Lasso) regression.[30] The details of the Lasso regression have been described elsewhere.[31,32] In brief, Lasso is a shrinkage method for multivariate linear regression, and the sum of the absolute values of the regression coefficients is penalized. With Lasso regression, the prediction error was calculated through leave-one-out cross-validation, in which a single eye's data were used as the testing dataset and the remaining data were used as training data. This procedure was repeated such that every eye in the original sample was used just once as testing data; thus, for each individual, a diagnosis was produced using the data from all other subjects ($n = 42$ of 43). The λ value, the degree of penalty in Lasso, which provided non-zero coefficients to 20 variables, was identified and these 20 variables were regarded as candidate variables. Second, the model selection used to identify the optimal model for the PRAA was carried out using the second-order bias-corrected Akaike information criterion (AICc) index, from all 2^{20} patterns using the 20 candidate variables. The AIC is a well-known statistical measurement used in model selection, and the AICc is a corrected version of the AIC, which provides an accurate estimation even when the sample size is small.[33] The marginal R-squared (mR^2) value was calculated following a method proposed by

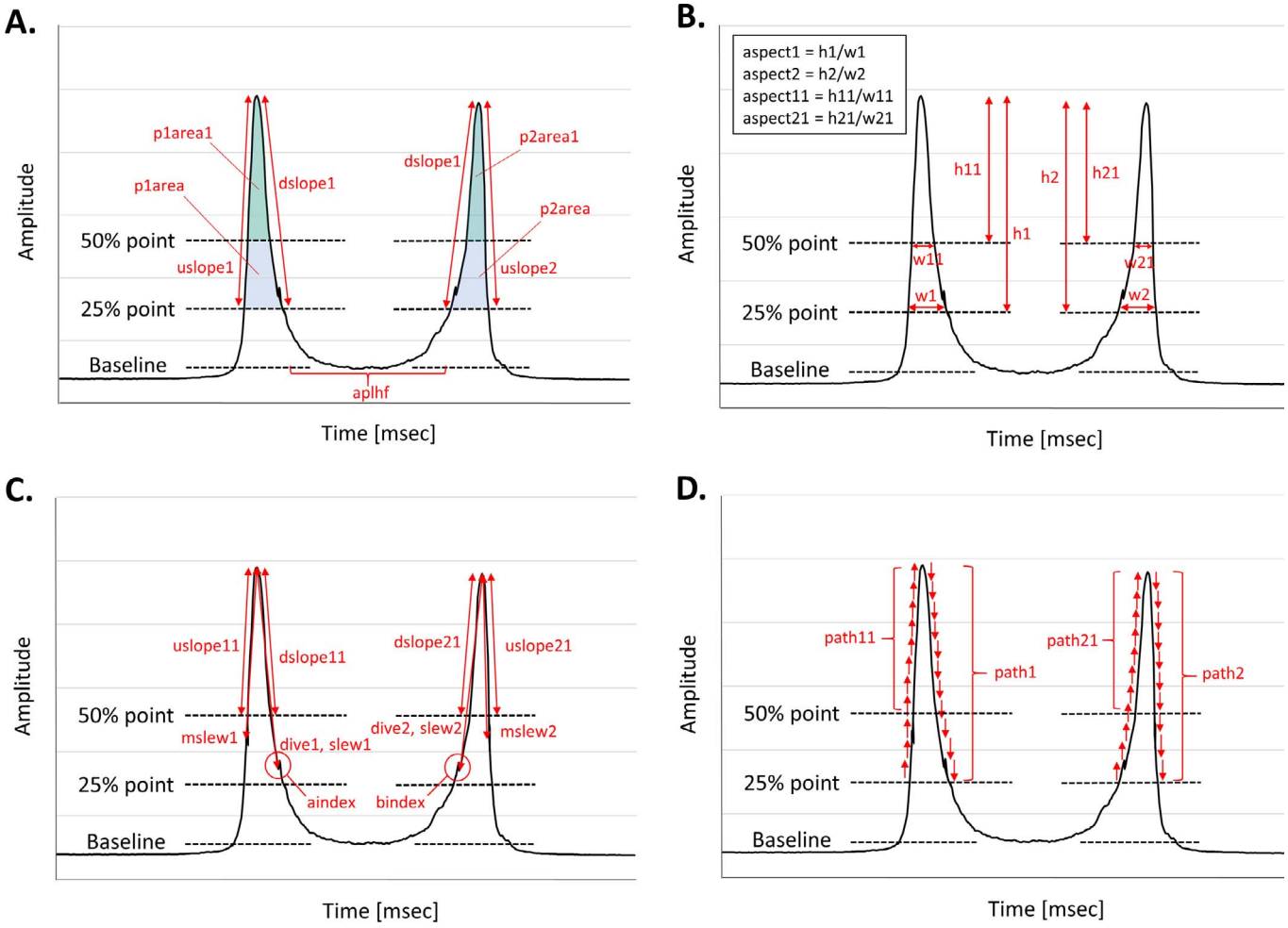

Figure 2. ORA waveform parameters. The ORA waveform is composed of two peaks, the inward-signal peak (peak 1, left) and outward-signal peak (peak 2, right). ORA waveform parameters consist of 37 parameters, which represent characteristics of these two ORA response wave peaks. These parameters are defined as height, width, degree, length, area, aspect ratio, and degree of non-monotonicity of the two peaks, and frequency noise between the two peaks. (A) p1area, p2area, p1area1, p2area1, uslope1, uslope2, dslope1, dslope2, and aplhf. (B) h1, h2, h11, h21, w1, w2, w11, w21, aspect1, aspect2, aspect11, and aspect21. (C) uslope11, uslope21, dslope11, dslope21, mslew1, mslew2, dive1, dive2, slew1, slew2, aindex, and bindex. (D) path1, path2, path11, and path21.

Nakagawa and Schielzeth.[34] Then, the log-likelihood of a paired model was compared using the analysis of variance (ANOVA) test.

All statistical analyses were performed using R (version 3.4.3, http://www.R-project.org/). The Lasso regression were calculated using the R package "glmnet." A linear mixed model was used to analyze the relationship between variables, whereby patients were regarded as a random effect.

Results

The demographics of the eyes are shown in Table 1. Table 2 shows summary of the statistics of corneal biomechanical properties.

A large SERE error was significantly correlated with large PRAA (coefficient = 1.77, standard error [SE] = 0.82, mR^2 = 0.10, P = 0.038, linear mixed model) (Fig. 3A). The relationship between AL and

Table 1. Demographic Data of the Subjects

Variables	Mean ± Standard Deviation (Range)
Age, y	53.7 ± 21 (26–85)
Sex (male/female)	21/20
AL, mm	24.1 ± 1.3 (21.5–27.1)
Spherical equivalent	−0.43 ± 2.5 (−5.8 to 4.1)
Keratometry, mm	8.2 ± 0.5 (7.4–9.2)
PPRA, degrees	138.7 ± 13.9 (106.9–172.0)

Table 2. Summary Statistics of ORA Parameters

Variables	Mean ± Standard Deviation (Range)
CH, mm Hg	10.15 ± 0.9 (8.24–12.09)
CRF, mm Hg	9.67 ± 1.2 (7.20–12.33)
aindex	9.95 ± 0.21 (8.78–10)
bindex	9.63 ± 0.75 (5.69–10)
p1area	7827.15 ± 1460.72 (5385.04–12026.31)
p2area	5777.48 ± 1300.87 (3626.50–8540.52)
aspect1	26.38 ± 2.91 (19.01–31.98)
aspect2	22.37 ± 4.02 (13.78–29.44)
uslope1	83.96 ± 11.54 (61.62–104.28)
uslope2	80.77 ± 16.59 (42.61–113.34)
dslope1	39.36 ± 4.88 (28.07–51.25)
dslope2	32.54 ± 6.11 (18.98–43.02)
w1	24.22 ± 2.79 (19.33–32.67)
w2	24.40 ± 3.27 (18.67–32)
h1	629.16 ± 29.80 (487.13–673.38)
h2	525.83 ± 71.62 (395.63–652.75)
dive1	587.50 ± 35.61 (425.75–640.58)
dive2	481.01 ± 81.19 (278.25–631.67)
path1	15.97 ± 2.35 (10.29–20.49)
path2	18.43 ± 3.28 (13.39–32.33)
mslew1	163.94 ± 23.82 (97–213.42)
mslew2	136.48 ± 28.13 (87.33–207.17)
slew1	84.03 ± 11.41 (62.22–104.28)
slew2	81.88 ± 16.09 (47.29–113.34)
aplhf	0.82 ± 0.25 (0.5–2.17)
p1area1	3903.64 ± 892.60 (2497.42–6567.63)
p2area1	2668.89 ± 680.09 (1457.50–4053.08)
aspect11	29.73 ± 4.22 (19.19–36.73)
aspect21	28.04 ± 5.64 (19.63–46.92)
uslope11	73.17 ± 13.29 (46.74–100.47)
uslope21	73.38 ± 14.35 (42.36–106)
dslope11	47.76 ± 6.97 (30.07–60.08)
dslope21	44.72 ± 9.25 (28.92–72.57)
w11	14.50 ± 2.35 (11.33–21.67)
w21	13.22 ± 2.21 (7.33–19.67)
h11	419.44 ± 19.87 (324.75–448.92)
h21	350.55 ± 47.74 (263.75–435.17)
path11	20.15 ± 3.68 (12.02–27.47)
path21	24.69 ± 4.09 (16.65–35.04)
Quality index	8.85 ± 0.6 (7.58–9.70)

PRAA approached significance (coefficient = −3.04, standard error = 1.63, mR^2 = 0.077, P = 0.070, linear mixed model) (Fig. 3B). There was no significant relationship between AL and CH (P = 0.50, linear mixed model).

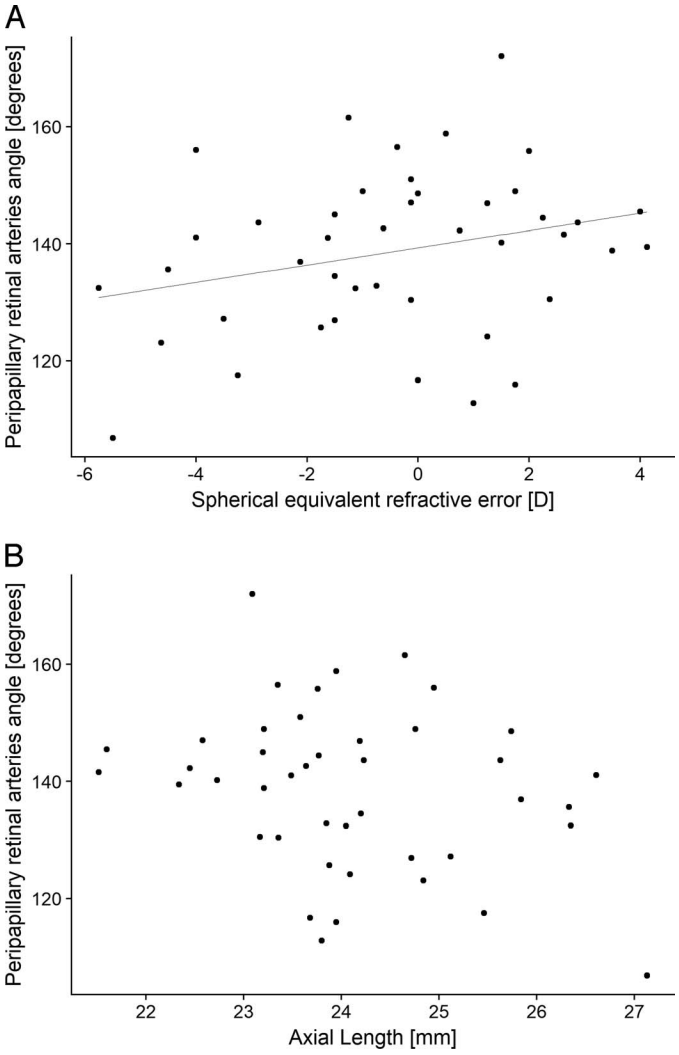

Figure 3. (A) Relationship between SERE and PRAA. SERE significantly decreased with the increase of PRAA (P = 0.038, linear mixed model). (B) Relationship between AL and PRAA. The relationship between AL and PRAA approached significance (P = 0.070, linear mixed model).

Lasso regression resulted in 20 provisional variables of keratometry, AL, CRF, aindex, bindex, aspect2, dslope1, w1, w2, h1, dive2, mslew1, slew1, aplhf, p2area1, dslope11, w11, w21, path11, and path21. The relationships between PRAA and the values of age, AL, CH, CRF, SERE, and the 35 ORA waveform parameters were calculated with the univariate linear mixed model (Table 3).

The optimal linear model with AICc model selection for the PRAA was the following: PRAA = 68.6–3.0 (SE = 1.5, P = 0.059) × AL − 3.1 (SE = 1.6, P = 0.055) × CRF + 9.5 (SE = 1.1, P < 0.0001) × aindex

Table 3. Results of Univariate Analyses Between PRAAs and the Values of Age, AL, CH, CRF, SERE, and 35 ORA Waveform Parameters

Variables	Coefficient	SE	*P*	AICc
Age	0.10	0.10	0.34	352.2
AL	−3.04	1.63	0.070	344.2
CH	−3.06	2.25	0.19	345.5
CRF	−3.50	1.73	0.050	343.6
SERE	1.77	0.82	0.038*	344.5
aindex	5.87	5.88	0.44	344.1
bindex	−2.40	2.84	0.40	345.8
p1area	−0.0015	0.0015	0.33	360.7
p2area	−0.0012	0.0016	0.46	360.9
aspect1	0.71	0.61	0.28	347.6
aspect2	−0.78	0.50	0.13	349.8
uslope1	0.28	0.19	0.15	349.8
uslope2	−0.28	0.12	0.027*	348.0
dslope1	0.33	0.34	0.37	349.8
dslope2	−0.32	0.33	0.33	349.9
w1	−0.72	0.70	0.32	348.2
w2	0.54	0.62	0.39	348.8
h1	0.017	0.071	0.81	353.8
h2	−0.051	0.029	0.083	353.1
dive1	0.013	0.061	0.83	354.1
dive2	−0.056	0.025	0.035*	351.8
path1	1.27	0.92	0.17	346.9
path2	−0.35	0.64	0.59	349.2
mslew1	−0.11	0.089	0.21	351.9
mslew2	−0.11	0.073	0.15	351.8
slew1	0.28	0.19	0.15	349.8
slew2	−0.24	0.13	0.065	349.2
aplhf	−2.82	7.87	0.72	344.3
p1area1	−0.0024	0.0024	0.34	359.8
p2area1	−0.0028	0.0030	0.36	359.3
aspect11	0.72	0.46	0.14	347.7
aspect21	−0.48	0.37	0.20	348.9
uslope11	0.29	0.16	0.081	349.1
uslope21	−0.20	0.15	0.19	350.7
dslope11	0.38	0.28	0.19	349.3
dslope21	−0.20	0.23	0.41	350.8
w11	−1.16	0.86	0.19	347.1
w21	0.76	0.96	0.43	348.0
path11	0.74	0.59	0.22	348.2
path21	0.14	0.50	0.78	349.9

* $P < 0.05$.

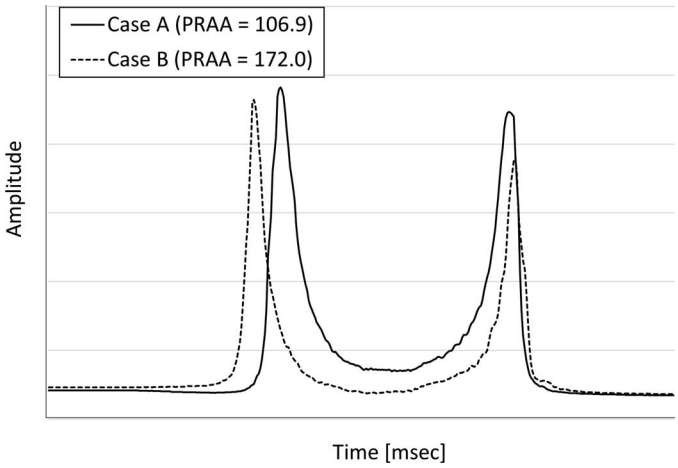

Figure 4. ORA waveform in example cases. ORA waveform with small PRAA (case A: *solid line*) and large PRAA (case B: *dashed line*) in example cases. PRAA, AL, CRF, aindex, w2, and slew1 in case A were 106.9 degrees, 27.1 mm, 11.8 mm Hg, 10, 26, and 86.3, respectively, whereas those values were 172.0 degrees, 23.1 mm, 8.5 mm Hg, 10, 23.7, and 91.2, respectively, in case B.

$+ 1.8$ (SE $= 0.09$, $P < 0.0001$) $\times$ w2 $+ 0.40$ (SE $= 0.18$, $P = 0.028$) $\times$ slew1 (AICc $= 334.6$, m$R^2 = 0.29$).

The log-likelihood of this optimal model was significantly better (all $P < 0.0001$, ANOVA) than those with the AL-only model (AICc $= 344.2$, m$R^2 = 0.08$), the model only with CH (AICc $= 345.5$, m$R^2 = 0.04$), the model only with CRF (AICc $= 343.6$, m$R^2 = 0.09$), the model with AL and CH (AICc $= 342.6$, m$R^2 = 0.09$), and the model with AL and CRF (AICc $= 341.0$, m$R^2 = 0.14$). There was no significant difference in the log-likelihoods of the AL-only model and the model with AL and CH, and the AL-only model and the model with AL and CRF ($P = 0.42$ and 0.09, respectively, ANOVA).

Figure 4 shows the ORA waveform with small PRAA (case A) and large PRAA (case B) as example cases. PRAA, AL, CRF, aindex, w2, and slew1 in case A were 106.9 degrees, 27.1 mm, 11.8 mm Hg, 10, 26, and 86.3, respectively, whereas those values were 172.0 degrees, 23.1 mm, 8.5 mm Hg, 10, 23.7, and 91.2, respectively, in case B.

Discussion

In this study, the relationship between the PRAA and corneal biomechanical properties, including the ORA waveform parameters, were evaluated in healthy eyes. As a result, the PRAA was best described using the ORA waveform parameters in

combination with AL and CRF; CH was not included in this optimal model.

We have previously reported that the increase of AL is significantly ($P = 0.006$) related to the decrease of the PRAA.[11] In the current study, long AL tended to be related to small PRAA, but this relationship merely approached significance ($mR^2 = 0.077$, $P = 0.070$). This difference could be attributed to the difference of the nature of the studied eyes; in our previous study, eyes with high myopia were included, whereas the inclusion criterion in the current study was SERE larger than −6.0 D. In the previous study, the correlation between AL and the PRAA was merely moderate ($R = -0.38$), even in highly myopic eyes. The PRAA represents the magnitude of retinal stretch associated with the elongation of the eyeball, and these results suggested that AL alone was not sufficient to represent the retinal stretch, in particular in eyes with high myopia (SERE < -6.0 D).

In contrast, the current results suggested retinal stretch estimated by the PRAA was much better described by using the ORA waveform parameters ($mR^2 = 0.29$) compared with AL alone. The ORA uses a measurement of corneal response to external energy (air puff); however, cornea and sclera are intrinsically made up of the same types of collagen,[35] which implies these tissues share similar biomechanical properties. A previous study has suggested that CH decreases with an increase of AL.[36] However, this relationship was not observed in the current study ($P = 0.62$). Furthermore, the log-likelihood of the model with AL and CH, and the model with AL and CRF were not significantly different from that with the AL-only model. These results suggested that the biomechanical change in retina due to the elongation of the eye was more precisely represented with detailed analysis of the ORA waveform, and sensitively reflected by using the ORA waveform parameters than using (only) CH or CRF. ORA-CH and CRF are mainly derived from the pressure information during the ORA measurement (P1 and P2), whereas ORA waveform parameters represent the corneal deformation during the ORA measurement. Similar detailed observation of the shape of cornea following the application of air jet can also be made using the CST device. We recently reported that CST parameters are changed with elongation of an eye, which suggested the ability to absorb applied external energy is poor in eyes with narrower cpRNFL peak angles associated with the elongation of eyes.[15] Matalia et al.[37] also reported that, using CST, eyes with a corneal elastic modulus were decreased in eyes with high myopia. The selected ORA waveform parameters indicated that a short non-monotonicity in peak 1 (aindex), a narrow width of peak 2 (w2), and a steep inside slope of peak 1 (slew1) were associated with myopic eyes (small PRAA) in the current study. Such waveform parameters represent a quick response of cornea to external forces, which suggests a soft cornea.[38,39] This implies that ORA waveform parameters are useful to assess the myopic retinal changes; however, it is not straightforward to interpret these multiple parameters simultaneously, and further future examinations are needed.

A previous study shows that CRF was significantly lower in highly myopic eyes compared with emmetropic eyes,[40] although there is another study that suggested no relationship between AL and CRF.[41] In the current study, CRF increased with the decrease of PRAA. It should be noted that CRF may be a weaker predictor of PRAA than other selected waveform parameters, as suggested by the relatively large P value in the optimal model ($P = 0.055$). Corneal stiffness may change with aging; however, a previous Corvis ST study suggested that this effect is negligible.[42] Reflecting this, the variable of age was not selected in the optimal model for PRAA in the current study.

As previous studies indicated, corneal biomechanics are changed in highly myopic eyes.[36,37] However, highly myopic eyes were excluded in the current study because the main purpose was to investigate eyes within an ordinary status, which is the limitation of the current study. It would be of further interest to investigate the relationship between the ORA waveform parameters and the PRAA in highly myopic eyes, and a future study should be conducted shedding light on this issue.

In conclusion, the ORA waveform parameters were associated with myopic retinal stretch estimated by the PRAA, suggesting an alteration of biomechanical properties of the retina in elongated eyes.

Acknowledgments

Supported by grants from the Japan Science and Technology Agency (JST)-CREST and Grant 17K11418 from the Ministry of Education, Culture, Sports, Science and Technology of Japan.

Disclosure: **S. Asano**, None; **R. Asaoka**, None; **T. Yamashita**, None; **S. Aoki**, None; **M. Matsuura**,

None; **Y. Fujino**, None; **H. Murata**, None; **S. Nakakura**, None; **Y. Nakao**, None; **Y. Kiuchi**, None

References

1. Morgan IG, Ohno-Matsui K, Saw S-M. Myopia. *Lancet*. 2012;379:1739–1748.
2. Morgan I, Rose K. How genetic is school myopia? *Prog Retin Eye Res*. 2005;24:1–38.
3. Pan CW, Ramamurthy D, Saw SM. Worldwide prevalence and risk factors for myopia. *Ophthalmic Physiol Opt*. 2012;32:3–16.
4. Lin LL-K, Shih Y-F, Hsiao CK, Chen C. Prevalence of myopia in Taiwanese schoolchildren: 1983 to 2000. *Ann Acad Med Singapore*. 2004;33:27–33.
5. Sawada A, Tomidokoro A, Araie M, Iwase A, Yamamoto T, Group TS. Refractive errors in an elderly Japanese population: the Tajimi study. *Ophthalmology*. 2008;115:363–370.e363.
6. Ohsugi H, Ikuno Y, Shoujou T, Oshima K, Ohsugi E, Tabuchi H. Axial length changes in highly myopic eyes and influence of myopic macular complications in Japanese adults. *PLoS One*. 2017;12:e0180851.
7. Ogawa A, Tanaka M. The relationship between refractive errors and retinal detachment—analysis of 1,166 retinal detachment cases. *Jpn J Ophthalmol*. 1988;32:310–315.
8. Fang X, Weng Y, Xu S, et al. Optical coherence tomographic characteristics and surgical outcome of eyes with myopic foveoschisis. *Eye*. 2009;23:1336.
9. Lim R, Mitchell P, Cumming RG. Refractive associations with cataract: the blue mountains eye study. *Invest Ophthalmol Vis Sci*. 1999;40:3021–3026.
10. Mitchell P, Hourihan F, Sandbach J, Wang JJ. The relationship between glaucoma and myopia: the Blue Mountains Eye Study. *Ophthalmology*. 1999;106:2010–2015.
11. Yamashita T, Asaoka R, Tanaka M, et al. Relationship between position of peak retinal nerve fiber layer thickness and retinal arteries on sectoral retinal nerve fiber layer thickness. *Invest Ophthalmol Vis Sci*. 2013;54:5481–5488.
12. Yoo YC, Lee CM, Park JH. Changes in peripapillary retinal nerve fiber layer distribution by axial length. *Optom Vis Sci*. 2012;89:4–11.
13. Hong SW, Ahn MD, Kang SH, Im SK. Analysis of peripapillary retinal nerve fiber distribution in normal young adults. *Invest Ophthalmol Vis Sci*. 2010;51:3515–3523.
14. Axer-Siegel R, Herscovici Z, Davidson S, Linder N, Sherf I, Snir M. Early structural status of the eyes of healthy term neonates conceived by in vitro fertilization or conceived naturally. *Invest Ophthalmol Vis Sci*. 2007;48:5454–5458.
15. Matsuura M, Murata H, Nakakura S, et al. The relationship between retinal nerve fibre layer thickness profiles and CorvisST tonometry measured biomechanical properties in young healthy subjects. *Sci Rep*. 2017;7:414.
16. Jung Y, Park H-YL, Park CK. Association between corneal deformation amplitude and posterior pole profiles in primary open-angle glaucoma. *Ophthalmology*. 2016;123:959–964.
17. Jonas JB. Clinical implications of peripapillary atrophy in glaucoma. *Curr Opin Ophthalmol*. 2005;16:84–88.
18. Jonas JB, Fernández MC, Naumann GO. Glaucomatous parapapillary atrophy: occurrence and correlations. *Arch Ophthalmol*. 1992;110:214–222.
19. Kono Y, Zangwill L, Sample PA, et al. Relationship between parapapillary atrophy and visual field abnormality in primary open-angle glaucoma. *Am J Ophthalmol*. 1999;127:674–680.
20. Teng CC, De Moraes CG, Prata TS, et al. The region of largest β-zone parapapillary atrophy area predicts the location of most rapid visual field progression. *Ophthalmology*. 2011;118:2409–2413.
21. Asano S, Nakajima K, Kure K, et al. Corneal biomechanical properties are associated with the activity and prognosis of Angioid Streaks. *Sci Rep*. 2018;8:8130.
22. Hirasawa K, Matsuura M, Murata H, et al. Association between corneal biomechanical properties with ocular response analyzer and also CorvisST tonometry, and glaucomatous visual field severity. *Transl Vis Sci Technol*. 2017;6:18.
23. Aoki S, Murata H, Matsuura M, et al. The effect of air pulse-driven whole eye motion on the association between corneal hysteresis and glaucomatous visual field progression. *Sci Rep*. 2018;8:2969.
24. Hayes DD, Teng CC, de Moraes CG, Tello C, Liebmann JM, Ritch R. Corneal hysteresis and Beta-zone parapapillary atrophy. *Am J Ophthalmol*. 2012;153:358–362.e351.
25. Aoki S, Murata H, Matsuura M, et al. The relationship between the waveform parameters from the ocular response analyzer and the progression of glaucoma. *Ophthalmology Glaucoma*. 2018;1:123–131.

26. Littmann H. Zur Bestimmung der wahren Größe eines Objektes auf dem Hintergrund des lebenden Auges. *Klin Monbl Augenheilkd*. 1982;180:286–289.
27. Matsuura M, Hirasawa K, Murata H, et al. The relationship between Corvis ST tonometry and ocular response analyzer measurements in eyes with glaucoma. *PLoS One*. 2016;11:e0161742.
28. Dupps WJ Jr. Hysteresis: new mechanospeak for the ophthalmologist. *J Cataract Refract Surg*. 2007;33:1499–1501.
29. Pinero DP, Alcon N. Corneal biomechanics: a review. *Clin Exp Optom*. 2015;98:107–116.
30. Tibshirani R. Regression shrinkage and selection via the lasso. *J R Stat Soc Series B Stat Methodol*. 1996;58:267–288.
31. Fujino Y, Murata H, Mayama C, Asaoka R. Applying "Lasso" regression to predict future visual field progression in glaucoma patients. *Invest Ophthalmol Vis Sci*. 2015;56:2334–2339.
32. Fujino Y, Murata H, Mayama C, Matsuo H, Asaoka R. Applying "Lasso" regression to predict future glaucomatous visual field progression in the central 10 degrees. *J Glaucoma*. 2017;26:113–118.
33. Burnham KP, Anderson DR. Multimodel inference. *Sociol Methods Res*. 2016;33:261–304.
34. Nakagawa S, Schielzeth H. A general and simple method for obtaining R2 from generalized linear mixed-effects models. *Methods Ecol Evol*. 2013;4:133–142.
35. Harper AR, Summers JA. The dynamic sclera: extracellular matrix remodeling in normal ocular growth and myopia development. *Exp Eye Res*. 2015;133:100–111.
36. Wong YZ, Lam AK. The roles of cornea and axial length in corneal hysteresis among emmetropes and high myopes: a pilot study. *Curr Eye Res*. 2015;40:282–289.
37. Matalia J, Francis M, Gogri P, Panmand P, Matalia H, Roy AS. Correlation of corneal biomechanical stiffness with refractive error and ocular biometry in a pediatric population. *Cornea*. 2017;36:1221–1226.
38. Roberts CJ. Concepts and misconceptions in corneal biomechanics. *J Cataract Refract Surg*. 2014;40:862–869.
39. Kerautret J, Colin J, Touboul D, Roberts C. Biomechanical characteristics of the ectatic cornea. *J Cataract Refract Surg*. 2008;34:510–513.
40. Del Buey MA, Lavilla L, Ascaso FJ, Lanchares E, Huerva V, Cristóbal JA. Assessment of corneal biomechanical properties and intraocular pressure in myopic Spanish healthy population. *J Ophthalmol*. 2014;2014:905129.
41. Qiu K, Lu X, Zhang R, Wang G, Zhang M. Corneal biomechanics determination in healthy myopic subjects. *J Ophthalmol*. 2016;2016:2793516.
42. Matalia J, Francis M, Tejwani S, Dudeja G, Rajappa N, Roy AS. Role of age and myopia in simultaneous assessment of corneal and extraocular tissue stiffness by air-puff applanation. *J Refract Surg*. 2016;32:486–493.